J18.5

S-NPP CRIS FULL SPECTRAL RESOLUTION SDR PROCESSING AND DATA QUALITY ASSESSMENT

Yong Han[1*], Yong Chen[2], Xiaozheng Xiong[3] and Xin Jin[3]

[1]Center for Satellite Applications and Research, National Environmental Satellite, Data, and Information Service, NOAA, College Park, MD
[2]University of Maryland, College Park, MD
[3]Earth Resources Technology, Inc, Laurel, MD

1. INTRODUCTION

On December 4, 2014, the Cross-Track Infrared Sounder (CrIS) on board the Suomi National Polar-Orbiting Partnership (S-NPP) satellite was commanded to the Full Spectral Resolution (FSR) mode from the Normal Spectral Resolution (NSR) mode which had been in operation since the beginning of CrIS measurements in February 2012. On the FSR mode, the interferograms of the three spectral bands are recorded with the same Maximum Path Difference (MPD), while on the NSR mode, the interferograms in the Mid-wave (MW) and shortwave (SW) bands are recorded with MPDs at a half of and a quarter of the long-wave (LW) band MPD, respectively.

The interferogram measurements together with the calibration data are sent to the ground in the form of Raw Data Records (RDRs). The ground processing software converts the interferogram measurements into calibrated and geolocated radiance spectra in the form of Sensor Data Records (SDR). The SDR software has two packages, which share the same processing code. One package is for operational use, running on the Interface Data Processing Segment (IDPS). The other is the Algorithm Development Library (ADL). ADL uses file based inputs and outputs, while IDPS uses a Data Management Subsystem (DMS) to manage the inputs and outputs.

After the transition of the CrIS instrument from the NSR to FSR mode operation, the IDPS system continued to process the RDRs into NSR SDRs by truncating the MW and SW band data into the NSR interferograms and will remain doing so for the foreseeable future. Therefore, the spectral resolution of the SDR data archived on NOAA's Comprehensive Large Array-data Stewardship System (CLASS) remains unchanged. In order to provide FSR SDR data to the user community, an ADL based processing system was developed to transform the RDRs into FSR SDRs. The FSR processing system is based on the NSR IDPS CrIS SDR software of the version Mx8.5/Block2.0. For convenience, the baseline NSR software is referred as NSR-IDPS, while the FSR ADL processing system as FSR-ADL. The NOAA Center for Satellite Application and Research (STAR) is one of the sites that provide routine processing of the FSR data and makes the SDR data available to the public via the STAR FTP site: ftp://ftp2.star.nesdis.noaa.gov/smcd/xxiong/. The SDR file names are tagged with labels "star", "f" and "01", meaning the data are processed at the NOAA/STAR site with the full spectral resolution SDR software and algorithm version 1. Since the format and data fields of the SDR files have not been changed, the CrIS SDR User's Guide (Han et al., 2013a) written for the NSR SDRs still applies to the FSR SDR product, except the descriptions on the dimension and resolutions of the MW and SW bands.

This paper mainly documents the changes made to convert the NSR-IDPS code to the FSR-ADL code (version 1) for the FSR SDR processing, with a focus on the calibration algorithms.

2. CRIS SPECTRAL CHARACTERISTICS

The CrIS instrument measures interferograms. An example of measured interferograms is shown in Figure 1. The interferograms are sampled by the instrument A/D converters, triggered by the electrical pulses provided by the laser metrology. The Optical Path Difference (OPD) sampling interval is the half of the laser wavelength of about 1550 nm. The length of the recorded interferogram determines the spectral resolution defined as 1/MPD, where MPD is the maximum OPD of the interferogram. Figure 2 shows

*Corresponding Author address: Yong Han, NOAA/NESDIS/STAR, College Park, MD 20764; e-mail: yong.han@noaa.gov

the difference of the interferogram MPDs between the NSR and FSR operation modes.

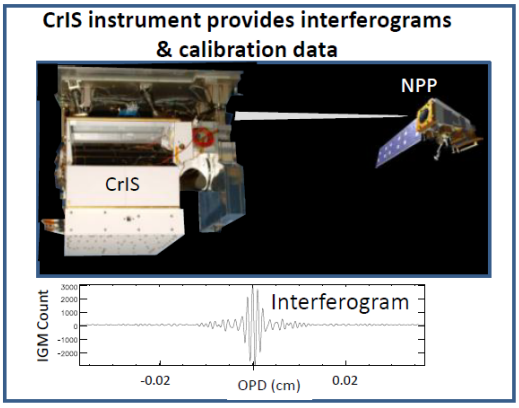

Figure 1. S-NPP CrIS interferogram measurement (only the central portion is shown)

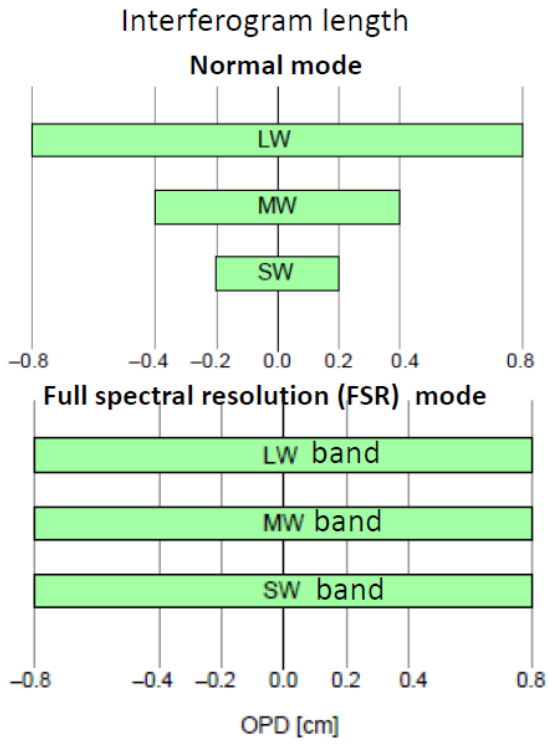

Figure 2. The CrIS double-side NSR and FSR mode interferogram OPDs.

The digitized interferogram measurements are further processed by a complex Finite Impulse Response (FIR) digital band-pass filter to reject out-band signals and its image pass band. In the FIR filtering process, the interferogram is also decimated with a decimation factor DF_b to reduce the number of interferogram data points from $N_{0,b}$ to N_b (the subscript *b* represents one of the three spectral bands). The interferogram measurement characteristics are summarized in Table 1.

The interferogram measurements together with the calibration data are sent to the ground for SDR processing to transform these measurements to calibrated spectra. Table 2 lists the spectral characteristics of the NSR and FSR mode spectra, and Figure 3 shows an example of measured FSR and NSR spectra generated by NSR-IDPS and FSR-ADL, respectively.

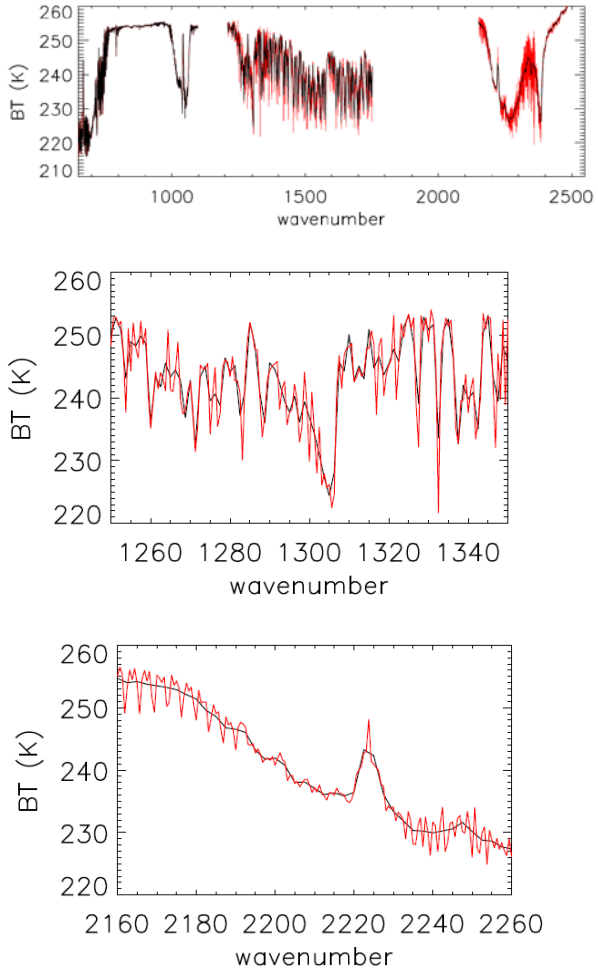

Figure 3. Example of calibrated NSR (black) and FSR (red) spectra (top panel) from the same interferogram measurement on December 4, 2014 after the CrIS was commanded to FSR mode operation. The middle and bottom panels are zoom-in of small portions of the spectra.

Table 1. CrIS NSR mode (black) and FSR mode (red) interferogram samples: numbers of interferogram samples spanning 2MPD before (column 2) and after (column 3) decimation, decimation factor (column 4) and MPD assuming an OPD sampling interval of 775 nm.

Band	$N_{0,b}$ (Un-decimated Samples spanning 2·MPD)	N_b (Samples after decimation)	DF_b (Decimation factor)	Radiometric MPD cm
LWIR	20736, 20736	864, 864	24, 24	0.8035, 0.8035
MWIR	21000,10560	1050, 528	20, 20	0.8138, 0.4092
SWIR	20722, 5 200	797, 200	26, 26	0.8049, 0.2015

Table 2. CrIS NSR mode (black) and FSR mode (red) SDR spectral characteristics. The in-band channels are those within the in-band spectral range. The guide bands include channels outside of the in-band spectral ranges and for each spectral band there are two guide bands on each end of the spectrum.

band	In-band spectral range (cm^{-1})	MPD (cm)	Resolution (cm^{-1})	Number of channels with guide bands	Number of in-band channels
LWIR	650-1095, 650-1095	0.8, 0.8	0.625, 0.625	864, 864	713, 713
MWIR	1210-1750, 1210-1750	0.8, 0.4	0.625, 1.25	1050, 528	865, 433
SWIR	2155-2550, 2155-2550	0.8, 0.2	0.625, 2.5	797, 200	633, 159

3. CALIBRATION ALGORITH UPDATES

Figure 4 shows the SDR processing algorithm flow, which applies to both NSR-IDPS and FSR_ADL processing systems. In other words, the algorithm module flow remains unchanged from the baseline code to the FSR code. The main components of the calibration algorithms include the Fast Fourier Transform (FFT) of the interferograms to raw spectra, detector nonlinearity (NL) correction, radiometric calibration, spectral calibration, and geolocation calculation, as well as the radiance noise estimation.

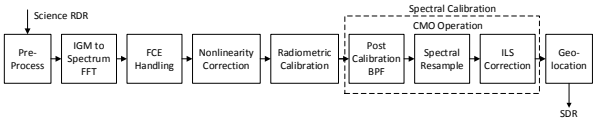

Figure 4. S-NPP CrIS SDR processing flow.

For both NSR-IDPS and FSR-ADL systems, the form of the calibration equation is given by Eq. (1), although some of the component algorithms differ:

$$S_{ES,Cal} = SA^{-1} \cdot F \cdot f \cdot \{\frac{S_{ES} - < S_{DS} >}{< S_{ICT} > - < S_{DS} >} B_{ICT}\} \cdot \qquad (1)$$

In the above calibration equation, the variables S_{ICT}, S_{DS} and S_{ES} are raw spectra of the Internal Calibration Target (ICT), Deep Space (DS) and Earth Scene (ES), the quantities inside of the angled brackets <…> are averages within the so-call sliding window (30 consecutive spectra), and B_{ICT}, f, $\boldsymbol{F}$ and $\boldsymbol{SA^{-1}}$ are the ICT radiance, post-filter, resampling matrix and self-apodization correction matrix (JPSS Configuration Management Office, 2011). The ICT radiance is computed using the Planck function with the self-apodization and contributions from ICT surrounding environment taking into account. The post-filter suppresses the noisy signals in the so-called guide bands that results from the radiometric calibration ratio in Eq. (1) (see Table 2 for in-band and guide-band definition). The resampling matrix performs two functions: a) changing the spectral resolution to the required resolution and b) interpolating the spectrum from the sensor grid to the required frequency grid. The self-apodization correction matrix corrects the spectral distortion due to radiance beam divergence effect. The three components, f, $\boldsymbol{F}$ and $\boldsymbol{SA^{-1}}$, are combined into a single matrix, referred as Correction Matrix Operator (CMO). In Eq. (1), the CMO is a component of spectral calibration and is used to perform spectral calibration, while the components in the brackets {…} together with the NL correction perform the radiometric calibration.

The NSR-IDPS algorithms and software were validated by the CrIS SDR Science team in the intensive Calibration and Validation (CalVal) process, which started near the beginning of the S-NPP mission in February of 2012 and ended in March of 2013 (Han et al., 2013b). The CalVal results are summarized in the five JGR papers (Han et al., 2013b; Strow et al., 2013; Tobin et al., 2013; Wang et al. 2013; and Zavyalov et al., 2013).

The CrIS SDR science team has been working to improve the SDR calibration algorithms. For FSR SDR processing, it has been found that some of the previous calibration algorithms, while working well for NSR SDR processing, do not produce acceptable results for the FSR SDR processing, and therefore must be changed or updated. In addition, changes to calibration algorithms were also made because they improve the calibration results. The main changes

made in converting the NSR-IDPS code to FSR-ADL code are in spectral calibration and radiance noise estimation algorithms, which are summarized below.

3.1 RESAMPLING ALGORITHM

The spectral bins of the raw spectra are equally spaced with a grid size equal to their spectral resolution $\Delta\sigma_b = 1/(N_b * DF_b * \lambda_s)$, where λ_s is the sampling interval of the interferogram and equals to half of the metrology laser wavelength. The laser wavelength varies slowly with time, resulting in the variation of the spectral resolution and grid size of the raw spectra. The function of the resampling algorithm is to compute the resampling matrix that maps the raw spectra to the specified (and fixed) spectral grids and resolution. The algorithm updates are summarized below.

The resampling matrices are re-computed for each Neon calibration. The peak-to-peak variation of the S-NPP metrology laser wavelength is about 3 ppm (10^{-4} %) per year. Since the resampling matrix is a function of the metrology laser wavelength, spectral errors will occur if the laser wavelength drifts away from the value used to compute the resampling matrix. To take the variation into account, the laser wavelength is periodically measured roughly once per orbit with a neon calibration system, using spectrally ultra stable neon emission lines. The NSR-IDPS processing software has been using a scheme that re-computes the resampling matrices whenever the cumulative variation of the metrology wavelength exceeds 2 ppm. This scheme is changed for FSR-ADL. The FSR-ADL software re-computes the resampling matrix for each neon calibration, which reduces spectral calibration uncertainty up to 2 ppm.

Un-decimated bin size $N_{0,b}$ is used in resampling matrix calculation. The resampling matrix is computed with the following equation,

$$F_b[k,k'] = \frac{\Delta\sigma_b}{\Delta\sigma_b^{\,u}} \frac{Sinc(\frac{\sigma_{k'} - \sigma_k^{\,u}}{\Delta\sigma_b^{\,u}})}{Sinc(\frac{\sigma_{k'} - \sigma_k}{N\Delta\sigma_b^{\,u}})}. \qquad (2)$$

In Eq. (2), Sinc() is the Sinc function, $\Delta\sigma_b$ and $\Delta\sigma_b^{\,u}$ are spectral resolutions of the raw spectrum on the sensor grid determined by the metrology laser wavelength and of the resulting spectrum on the specified grid (user grid), respectively, and $\sigma_{k'}$ and $\sigma_k^{\,u}$ are the wavenumbers for the k'-th bin of the spectrum on the sensor grid and k-th bin of the spectrum on the user grid. In FSR-ADL processing, the number N in Eq. (2) equals to $N_{0,b}$, which is the size of the interferogram before decimation, while in NSR-IDPS processing, the number N equals to N_b, which is the size of the interferogram after decimation (see Table 1 for the values of $N_{0,b}$ and N_b). Eq. (2) with $N = N_{0,b}$ is derived in the un-decimated interferogram domains and the results are consistent with the Sinc channel spectral response function defined for the SDR radiance product.

3.2 SELF-APODIZATION MATRIX ALGORITHM

The self-apodiztion correction matrix $\boldsymbol{SA^{-1}}$ has a dimension of N_b x N_b. It is the inverse of the self-apodiztion matrix ***SA***. In both FSR-ADL and NSR-IDPS systems, ***SA*** is computed in the un-decimated spectral domains (JPSS Configuration Management Office, 2011). The dimension size of the matrix ***SA*** is optimized to balance the computational efficiency and energy conservation that requires the summation of the column of the SA matrix equal to one. The dimension size is given by N_b*r, where r is the expansion factor. For NSR-IDPS, r takes the value of 1.1 for all spectral bands. While this value is adequate for the NSR processing, it is too small for FSR processing to preserve energy on the MW and SW bands. Numerical experiments were conducted to optimize the expansion factors for FSR processing. The three expansion factors were determined as 1.4, 2.0 and 2.0 for the LW, MW and SW bands, respectively. After the matrix inverse operation for ***SA***, the matrix $\boldsymbol{SA^{-1}}$ is trimmed to the desired size. Figure 5 shows a comparison of the SW band spectra calibrated using the original expansion factor 1.1 and the new expansion factors. With this change, the ringing artifacts that appear in the spectrum calibrated with the original expansion factor are effectively eliminated.

3.3 CMO HANDLING

The Correction Matrix Operator (CMO) is a matrix that combines the three spectral calibration components $\boldsymbol{SA^{-1}}$, ***F*** and f used in Eq. (1). In NSR-IDPS processing, the CMO matrices are loaded from a CMO file. If the variation of the metrology laser wavelength exceeds 2 ppm, they are recomputed and then saved. In FSR SDR processing, only the $\boldsymbol{SA^{-1}}$ matrices are stored in the file, which do not need to be updated because they are constant. The CMO matrix is dynamically generated by combining the $\boldsymbol{SA^{-1}}$ matrix with the resampling matrix ***F*** and post-filter f.

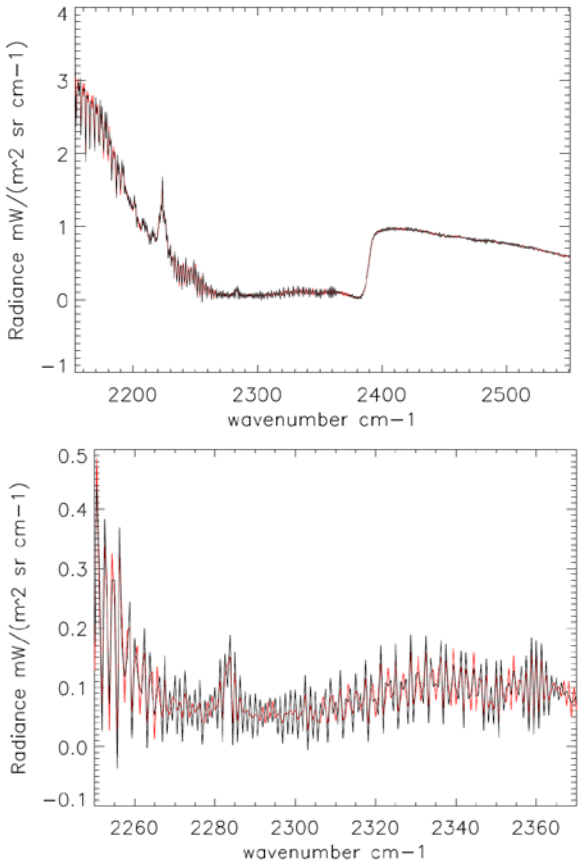

Figure 5. Shortwave band spectra processed with an expansion factor 1.1 (black) and 2.0 (red). The bottom panel is a zoom-in of a portion of the spectra shown in the top panel.

3.4 NEDN ALGORITHM

The radiance noise level is measured with the Noise Equivalent Differential Radiance (NEdN), computed as the standard deviation of calibrated ICT spectra within the sliding window. In NSR-IDPS processing, the ICT spectra used for computing NEdN are not spectrally calibrated (the CMO matrices are not applied) in order to reduce the computational cost. This simplified NEdN estimation algorithm works fine for NSR SDRs since the NEdN difference between that with and without the CMO correction is small. However, for FSR SDRs, it was found that the noise levels and noise correlations between adjacent channels were significantly increased on the MW and SW bands by the self-apodization correction, as shown in Figure 6. Therefore, the CMO correction must be included in the NEdN calculations to take the noise effect into account. It should be pointed out that the CMO-introduced noise increase is in addition to the noise increase in the MW and SW bands due to the increase of spectral resolutions.

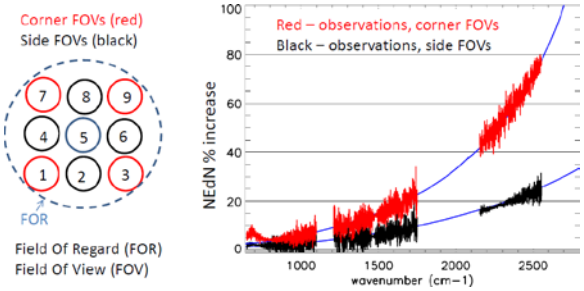

Figure 6. Field-of-views of the 3 x 3 detector arrays on the Earth surface (left), and the percentage increase of the NEdN due to self-apodiztion correction (right).

4. PRELIMINARY ASSESSMENT OF SDR QUALITY

The radiometric uncertainty (RU) of the NSR-IDPS processing has been evaluated and summarized in Tobin et al., 2013. Since the same radiometric calibration algorithms and NL correction coefficients are used in the FSR-ADL system, similar RU characteristics are expected for the FSR SDR processing. Figure 7 shows the radiance bias and standard deviation against the simulations for a full day of FSR SDR data set. The simulations were computed with the Community Radiative Transfer Model (CRTM) (Han, et al., 2006) with collocated ECMWF atmospheric profiles as inputs under the conditions of clear-sky and over ocean surface. The pattern and values of the bias and standard deviation are very similar to those obtained from the NSR SDRs processed by NSR-IDPS.

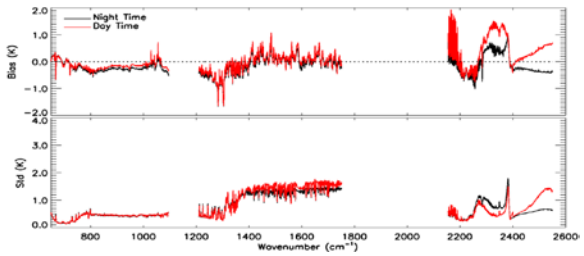

Figure 7. Radiance bias and standard deviation with respect to RTM simulation under clear-sky condition and over ocean for a full day measurements. Black – nighttime; red – daytime. The large bias during daytime at the 4.3 μm CO_2 absorption region is mainly due to the error of the RT model handling of Non-local Thermodynamic Equilibrium (NLTE).

In spectral (frequency) calibration, small improvement up to 2 ppm in the spectral frequency accuracy is expected due to more frequent updates of the resampling matrices that take the variation of the metrology laser wavelength into account. Figure 8 shows spectral uncertainty, estimated using the method (Chen et al., 2013; Straw et al., 2013) that maximizes the correlation between the measured spectra and the simulations computed with CRTM and ECMWF profiles. The absolute uncertainties of the spectral frequencies are less than 3 ppm as shown in Figure 8. The corresponding radiance error resulted from a 3 ppm channel frequency shift is frequency dependent and is less than 0.1 K in general. Also shown in Figure 8 is the relative frequency uncertainty, which is the spectral channel frequency shift relative to the spectra from detector FOV-5, the center FOV in the focal plane. The center FOV is less affected by the self-apodization.

The radiance noise levels are significantly increased in MW and SW bands for two reasons. One is the increase of the spectral resolution in the MW and SW bands, which results in noise increase by a factor 1.4 in MW band and 2.0 in SW band. The other reason, as described earlier in Section 3.4, is the self-apodization correction, which results in noise increase by up to 20% in the MW band and up to 78% in the SW band, depending on the FOV position and channel frequency. The figure in the top panel of Figure 9 shows an example of the FSR NEdN spectra. As shown in the figure, the NEdN curves spread among different FOVs, especially on the SW band. The main reason causing the spread is the self-apodization correction (see Section 3.4). Note that for both NSR-IDPS and FSR-ADL processing, the radiance spectra contained in SDRs are unapodized. However, most users apodize the radiance spectra before using them in order to reduce the side-lobes of the channel response function. The user apodization will reduce noise level by an amount depending on the type of Apodization function applied. The figure in the bottom panel of Figure 9 shows the NEdN spectra computed from Hamming-function apodized spectra. It is interesting to see that the Hamming apodization almost completely removes the portion of noise and noise spread introduced by the self-apodization correction. This result has been understood, and due to the space limitation of this paper, it will not be discussed here.

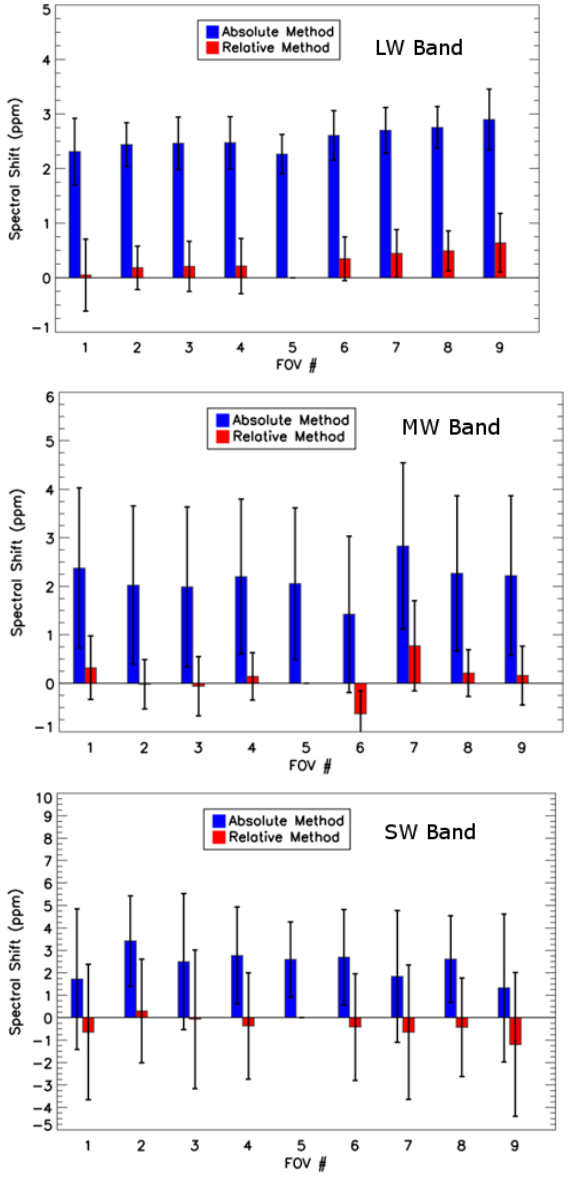

Figure 8. Absolute (blue) and relative (red) uncertainties of the channel center frequency assessed with an RT model and NWP profiles. The three figures correspond to the LW, MW and SW bands

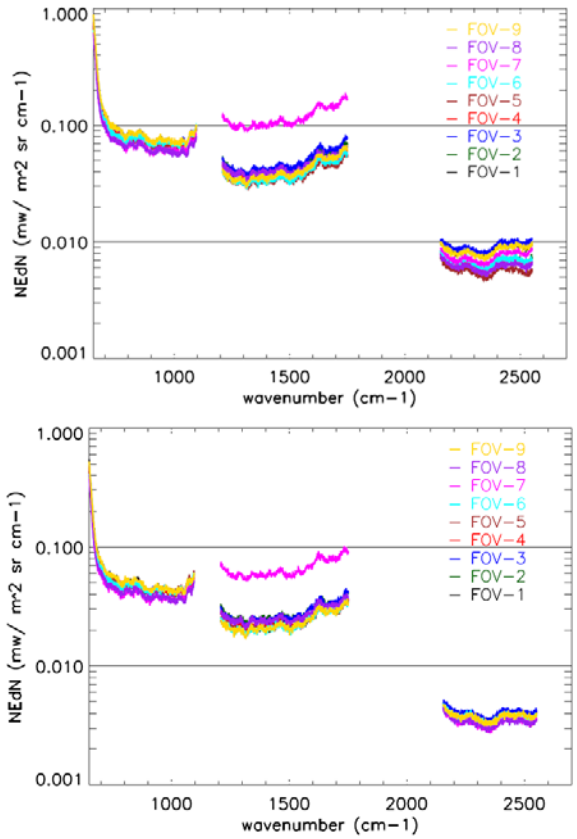

Figure 9. NEdN spectra of the unapodized spectra (top panel) and Hamming-apodized spectra (bottom panel). The spread of the NEdN among FOVs in unapodized spectra is due to the SA correction (see Figure 6), which is almost completely removed by Hamming apodiztion.

The overall status of every radiance spectrum is given by the overall quality flag, which has three values: Good, Degraded and Invalid. The numbers of spectra with Degraded or Invalid status are very small and are similar to the NSR-IDPS processing (Han et al., 2013b). The daily occurrence of the Degraded and Invalid spectra is less than 0.1% of the total number of the spectra. Figure 10a shows an example of the MW band water vapor channel 1500 cm^{-1} radiance image and Figure 10b shows the overall quality flag for the MW band spectra.

5. SUMMARY AND FUTURE WORK

An ADL based CrIS FSR SDR processing system was developed based on the IDPS source code Mx8.5/Block2.0. NOAA/STAR has been using the system to process the FSR RDRs into FSR SDRs available to the public. This paper documents the SDR algorithms implemented in the system with a focus on its algorithm differences from the well documented baseline software that has been used operationally to provide NSR SDRs. The most significant differences are mainly in the spectral calibration and NEdN estimation, as described in details in Section 3. The changes made to the spectral calibration algorithms improve the spectral frequency accuracy and reduces spectral ringing artifacts. The NEdN algorithm was modified to take into account of the noise increase due to the self-apodiztion correction, which is significant in the MW and SW bands. The SDR calibration equation, ILS parameters and neon wavelength for spectral calibration, NL correction algorithm and coefficients for radiometric calibration, and data quality control algorithms remain the same as in the baseline code.

The CrIS SDR team has been working to improve the calibration algorithms, including optimization of the calibration equation. Progress has been made and the preliminary results show significant improvement in ringing artifact reduction. We will implement these algorithm updates into the FSR-ADL system once they are finalized. Work is also underway in further assessment of the spectral and radiometric accuracies of the SDR product from the FSR processing system.

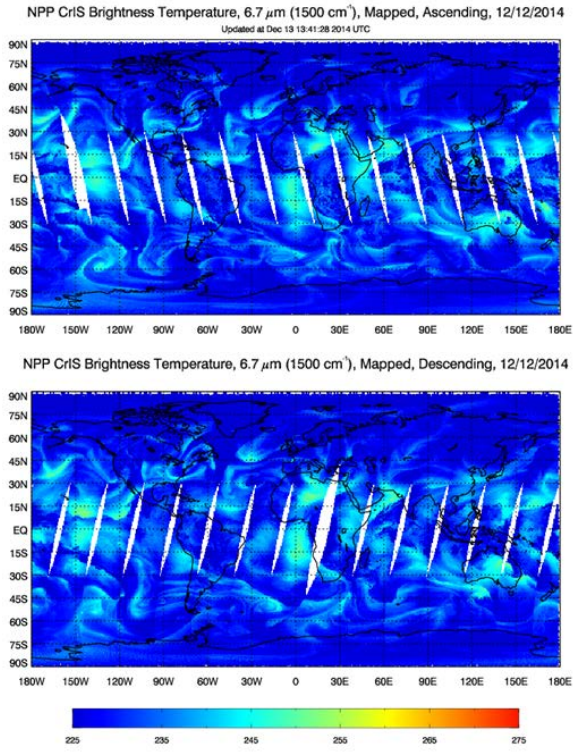

Figure 10a. Brightness temperature of the MW water vapor channel 1500 cm^{-1} in ascending (top) and descending (bottom orbits).

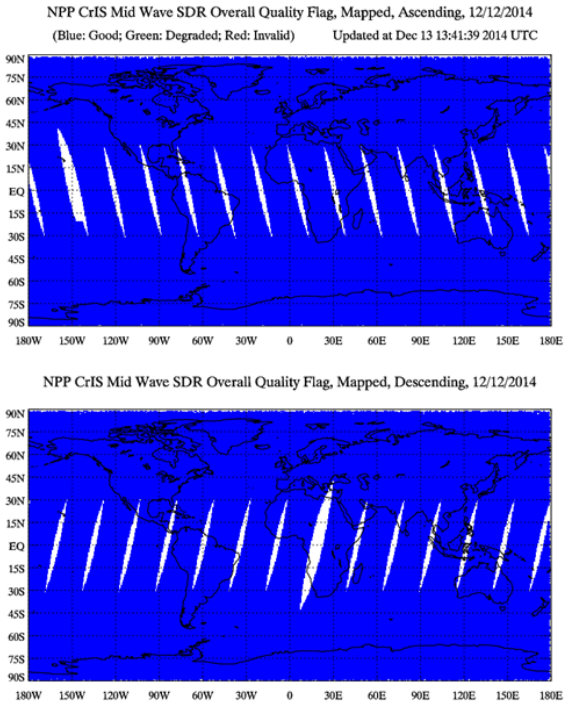

Figure 10b. MW band overall quality flag, associated with each spectrum. Blue – Good; Green – Degraded; and Red – Invalid.

ACKNOWLEDGMENT

This work was supported by JPSS program. The authors thank to the CrIS SDR Science team members for their contributions in SDR algorithm development and validations. The science team includes the groups of University of Wisconsin-Madison, led by H. Revercomb, University of Maryland at Baltimore County, led by L. Strow, Space Dynamics Laboratory, led by D. Scott, Massachusetts Institute of Technology, Lincoln Laboratory, led by D. Mooney, Exelis Inc., led by L. Suwinski, Northrop Grumman Aerospace Systems, led by D. Gu, NASA Langley Research Center, Led by D. Johnson, and members from NOAA/DESDIS/STAR.

REFERENCE

Chen, Y., Y. Han, and F. Weng, 2013: Detection of Earth-rotation Doppler shift from Suomi National Polar-Orbiting Partnership Cross-Track Infrared Sounder, *Appl. Opt.,* Vol. 52, No. 25, doi:10.1364/AO.52.006250

Han, Y., P. van Delst, Q. Liu, F. Weng, B. Yan, R. Treadon, and J. Derber, 2006: Community Radiative Transfer Model (CRTM) – Version 1. *NOAA NESDIS Technical Report* 122.

Han, Y., Y. Chen, X. Jin, D. Tremblay and L. Wang, 2013a: Cross Track Infrared Sounder (CrIS) Sensor Data Record (SDR) User's Guide – Version 1, *NOAA NESDIS Technical Report* 143.

Han, Y., et al., 2013b: Suomi NPP CrIS measurements, sensor data record algorithm, calibration and validation activities, and record data quality. *J. Geophys. Res. Atmos.,* 118, *doi:*10.1002/2013JD020344.

JPSS Configuration Management Office, 2011: Joint Polar Satellite System (JPSS) Cross Track Infrared Sounder (CrIS) Sensor Data Records (SDR) algorithm theoretical basis document (ATBD), *JPSS office, document code 474: 474-00032, October 2011*. [Available online at http://www.star.nesdis.noaa.gov/jpss/ATBD.php#S796056].

Strow, L. L., H. Motteler, D. Tobin, H. Revercomb, S. Hannon, H. Buijs, J. Predina, L. Suwinski, *and* R. Glumb, 2013: Spectral calibration and validation of the Cross–track Infrared Sounder (CrIS) on the Suomi NPP satellite. *J. Geophys. Res. Atmos.,* 118, *doi:*10.1002/2013JD020480.

Tobin, D., et al., 2013: Suomi-NPP CrIS radiometric calibration uncertainty. *J. Geophys. Res. Atmos.,* 118, 10,589–10,600, *doi:*10.1002/jgrd.50809.

Wang, L., D. A. Tremblay, Y. Han, M. Esplin, D. E. Hagan, J. Predina, L. Suwinski, X. Jin, *and* Y. Chen, 2013: Geolocation assessment for CrIS sensor data records, *J. Geophys. Res. Atmos.,* 118, *doi:*10.1002/2013JD020376.

Zavyalov, V., M. Esplin, D. Scott, B. Esplin, G. Bingham, E. Hoffman, C. Lietzke, J. Predina, R. Frain, L. Suwinski, Y. Han, C. Major, B. Graham, L. Phillips, 2013: Noise performance of the CrIS instrument, *J. Geophys. Res.*, doi: 10.1002/2013JD020457.